# Synthesis of microporous magnetic activated carbon from *Vicia faba* L. peels via FeCl₃-activation for efficient elimination of pollutants from liquid phase: Equilibrium and kinetics studies

Hajir M. Al-Khayat[1], Abdelrahman B. Fadhil[1*] 

[1] Department of Chemistry, College of Science, University of Mosul, Majmoaa Street, 41001, Mosul, Iraq
* Corresponding author's e-mail: abdelrahmanbasil@uomosul.edu.iq

## ABSTRACT

A one-step FeCl₃-facilitated carbonization/activation of a new precursor, namely *Vicia faba* L. Peels (VFPs), was developed to synthesize a novel microporous magnetic activated carbon (MMAC) for efficient elimination of methylene blue dye (MB) from wastewater and dibenzothiophene (DBT) from model fuel. The typical MMAC was produced using a 1.5:1 FeCl₃:VFPs impregnation ratio at 750 °C for 90 minutes, with a 10 °C/min heating rate. This adsorbent was characterized using various techniques (XRD, FESEM, EDX, N₂ adsorption-desorption, and VSM) to assess its crystallinity, morphology, texture, and magnetic properties. The BET surface area of the produced MMAC was 1224.80 m²/g, with a mean pore diameter of 1.91 nm. The VSM measurements confirmed the magnetic features of the resulting adsorbent, with a magnetization of 0.085 emu/g. The superior elimination of MB from its aqueous phase (200 mg/L) using the resulting MMAC reached 99.30% with 0.15 g of MMAC at 30 °C for 50 minutes and a pH of 9.0. At the same time, the maximum removal of the sulfur compound from the model (200 mg/L) amounted to 97.93% using 0.35 g of MMAC at 30 °C for 40 minutes. The adsorption of both contaminants from their liquid phases was better described by the Langmuir isotherm and the pseudo-2ⁿᵈ-order kinetic model than by other models. The maximum adsorptive capacity for MB was 331.50 mg/g compared with 31.83 mg/g for DBT at the typical working variables. Under typical experimental conditions, desulfurization of real oil fuel amounted to 62.22%. At the same time, the elimination of MB from its solutions in river and well waters was91.04% and 80.12%, respectively. Reusability of the studied pollutants over the regenerated adsorbent under the optimal working conditions exhibited an elimination performance of both contaminants above 90%. In conclusion, using agricultural solid waste for the eco-friendly preparation of novel adsorbents promotes sustainability and effective waste management.

**Keywords:** microporous magnetic activated carbon, adsorption of methylene blue and dibenzothiophene, isotherm and kinetic studies, reusability.

## INTRODUCTION

In recent decades, effective cleanup of industrial effluent has become a major challenge. Many countries now have stricter environmental rules and health quality standards. Toxic contaminants that defy traditional wastewater treatment methods are common in these effluents. Consequently, there is a significant effort to develop the strategies to remove these pollutants effectively (Zazo et al., 2012). Organic dyes have recently been employed as coloring in a wide range of industries, including textiles, plastics, paper, food, and cosmetics (Cheruiyot et al., 2019). The demand of enterprises for synthetic dyes continues to grow. Contaminated wastewater containing colors has a direct impact on living creatures and is a serious environmental issue (Dalmaz and Özak, 2024). Excessive exposure to organic dyes can adversely affect the eyes, neurological system, and cause vomiting, discomfort, fever, difficulty breathing, as well as hypertension (Priyadharshini et al., 2022). Methylene blue (MB) is a popular cationic dye implemented for biological staining, printing, and dyeing. The accumulation of MB dye in water is associated with several issues,

such as influencing human wellness and aquatic life (Julinawati et al., 2025). Highlighting the importance of a practical approach to wastewater treatment containing MB dye is a key objective. Chemical techniques (adsorption, accelerated oxidation (ozonation), and coagulation/flocculation), along with biological, physical, and membrane filtering methods, have all been employed to remediate the waste containing synthetic dyes, including MB dye (Zakir et al., 2025). On the other hand, in recent years, there have been significant environmental issues owing to the extensive usage of petroleum products. The combustion of the latter releases harmful oxides of sulfur ($SO_x$) into the atmosphere. As a result, global environmental regulatory organizations have set a limit of 20 ppm for S-compounds in transportation fuels in an effort to protect the environment (Yaseen et al., 2021). Hydrodesulfurization (HDS) is the standard method for removing S-compounds from gasoline, kerosene, and diesel. However, this approach requires harsh reaction conditions to eliminate sterically hindered alkyl derivatives of dibenzothiophenes (DBT), which are present in these fuels (Yaseen et al., 2021; Saeed et al., 2024). Consequently, alternative desulfurization processes were employed to achieve this target, like HDS, extractive desulfurization (EDS), Oxidative desulfurization (ODS), precipitative desulfurization (PDS), adsorptive desulfurization (ADS), and biodesulfurization (BDS) (Saeed et al., 2024).

Adsorption proved its effectiveness in removing many pollutants from the liquid phase. Numerous adsorbents have been employed to eliminate MB dye from contaminated water and DBT from different oils. Nonetheless, activated carbon (AC) exhibited the superior adsorptive efficiency (AE) in eliminating varied contaminants from the liquid media, owing to its elevated surface area, in addition to its surface, which contains numerous useful functional groups that are involved in the AE of contaminants from the liquid phase (Hussein and Fadhil, 2021). Also, variation in its pore-size distribution makes AC a potential adsorbent for removing many pollutants from liquid media (Hussein and Fadhil, 2021).

A variety of carbonaceous materials, like rubber tires (Saleh and Danmaliki, 2016) and polymer residues (Al-Layla et al., 2024), besides lignocellulosic byproducts, including rice husks (Yerdauletov et al., 2023), animal bones (Djilani et al., 2016), and palm kernel shells (Zakir et al., 2025), as well as other carbonaceous materials were implemented in the manufacture of AC. However, the production of AC from bio-wastes has gained more attention, as solid bio-waste has the added benefit of being "zero-carbon," making it environmentally friendly. Carbon-based sorbents with a high specific surface area and oxygen-rich functional groups can be easily made from bio-waste, thereby improving their absorption and purification performance (Zhang et al., 2025). Synthesis of AC can be achieved via two routes: physical activation of the raw feed or its derived char in the presence of several gases, like steam, $N_2$, $CO_2$, or a mix of these gases. In contrast, in the chemical activation, the authentic precursor or its generated biochar is treated with some chemical agents, including sulfuric acid, KOH, NaOH, $K_2CO_3$, $ZnCl_2$, $H_3PO_4$, or $FeCl_3$ (Harabi et al., 2024).

Compared with other chemical activation agents, such as KOH, $K_2CO_3$, $ZnCl_2$, and $H_3PO_4$, the use of $FeCl_3$ as an activating agent for AC is limited. Besides its chemical activating performance, this chemical adds a magnetic property to the resulting AC (Xu et al., 2020). In this regard, coffee husks were transformed into magnetic activated carbon (MAC) using $FeCl_3$ as an activating agent, and the resulting MAC had a surface area of 965 $m^2/g$, as established by Oliveira et al. (2009) (Oliveira et al., 2009). Ahmed (2011) investigated the preparation of AC via $FeCl_3$-activation, and the resulting adsorbent had a surface area of 1045.61 $m^2/g$ (Ahmed, 2011). The chemical activation of lignin by $FeCl_3$ produced a MAC with a surface area of 1150 $m^2/g$ and an adsorptive capacity of 300 mg/g for acetaminophen, as reported by Gomez-Aviles et al. (2022) (Gómez-Avilés et al., 2021). The waste cotton-derived textiles were chemically activated with $FeCl_3$ to create a MAC, which was used to purify wastewater from Cr (VI) (Xu et al., 2019). Shells of macadamia nut were converted into MAC via $FeCl_3$, and the resulting magnetic adsorbent was employed to eradicate 2,4-dichlorophenoxyacetic acid (Harabi et al., 2024). Lastly, sewage sludge was activated with $FeCl_3$, and the resulting magnetic adsorbent was utilized to purify wastewater from toxic Cr (VI) and As (III)(Shen et al., 2022). On the other hand, purification of transportation fuel from S-compounds using MAC has been established by several authors. In this regard, Fayazi et al. (2015) explored the elimination of DBT from model fuel over the AC/$\gamma$-$Fe_2O_3$ nanocomposite, which exhibited an adsorptive capacity of 38.0

mg/g (Fayazi et al., 2015). Razmi et al. (2025) studied the DS of DBT using a diesel model and waste-tire-derived pyrolytic oil over a hierarchical magnetic biochar. They reported an adsorption capacity of 134.14 mg/g (Razmi et al., 2025). Nonetheless, to the best of author's knowledge, one-step $FeCl_3$- activation of a novel feedstock, viz. *Vicia faba* L. Peels (VFPs) to synthesize a novel microporous magnetic activated carbon (MMAC) by adjusting the preparation conditions, has not been studied yet. Additionally, trying the typical MMAC in the removal efficiency (RE) of MB dye from the aqueous phase and DBT from model oil has not yet been established, as far as the authors know. These targets motivated us to conduct this study and bridge this gap.

Herein, a novel MMAC was developed from a new precursor, viz. VFPs via the optimized $FeCl_3$ activation approach. The resulting MMAC was implemented to eliminate the MB dye from wastewater and DBT from the model fuel by optimizing the adsorption process variables. Eliminating MB from river and well water solutions, and removing DBT from real fuel, was also explored. Investigations of the adsorption isotherms and kinetics were also conducted. Lastly, the reusability of the spent adsorbent was also tested.

## MATERIALS AND METHODS

### Precursors and chemicals

*Vicia faba* fruit was acquired at the local markets in Mosul city, Iraq. After the beans were separated from the skins, they were rinsed with distilled water (DW), dried under sunlight for 3 days, crushed, and screened to generate 100 mesh-sized particles. Adsorbates, i.e. MB ($C_{16}H_{18}ClN_3S$) and DBT ($C_{12}H_8S$) were acquired from Merck KGaA (Darmstadt, Germany). Chemicals, such as $FeCl_3.6H_2O$ (98.0–100.5%), HCl (36.5–38.0%), NaOH (98.50%), and DBT were supplied from Scharlab (Barcelona, Spain). These chemicals were used as received, without any prior preparation.

### $FeCl_3$-activation of VFPs

MMAC was synthesized from VFPs via a single-step $FeCl_3$ activation method. Initially, 5.0 g of the VFPs were mixed with the specified amount of the activator (1:1-3:1 $FeCl_3$: VFPs). After adding 50 mL of DW to the VFPs-$FeCl_3$

mixtures, which in turn were stirred for 5 h to ensure homogeneity, they were left overnight. The resulting blends were then dehydrated at 105 °C, followed by thermal activation in a muffle furnace (ISOLAB, Turkey) at various temperatures (550–950 °C) for different periods (30–120 minutes) at a constant rate of heating (10 °C/min). The activated samples were then extensively rinsed with HCl (0.1 N), followed by consecutive washing with DW till a pH of 6–7 was attained. Finally, the MMAC was oven-dried at 105 °C for 24h, crushed, and screened to obtain particles with a 100-mesh size. Optimizing the preparation conditions (amount of $FeCl_3$, temperature of activation, and the activation period) that affect the output and porosity of the resulting adsorbents. To explore the effect of each variable, the other parameters were held fixed. Each sample was prepared at least twice, and the results were provided as the average ± SD. The output of the produced MMAC samples was specified based on the following formula:

### Identification of the best MMAC

The $N_2$ adsorption/desorption isotherms at 77K were implemented to examine the pore structure, specific surface area, and pore size distribution of the produced MMAC using a surface area and porosity analyzer (BELSORP MINI II, Japan). The BET equation was adopted in measuring the specific surface area ($SA_{BET}$) of the as-created MMAC. Before conducting the adsorption-desorption process for the MMAC, the adsorbent was outgassed at 150 °C for 12 h to remove any adsorbed moisture from its surface. Determining the total pore volume ($V_{total}$) of the VFPs-derived MMAC was carried out at $P/P_o= 0.995$, while the average pore diameter ($d_{average}$) of MMAC was measured as per ($4V_{total}/S_{BET}$). Finally, the pore size distribution of the MMAC developed from VFPs was determined using the BJH method. Lastly, the resulting MMAC was assessed using its magnetization saturation curves, which were measured within ± 20 kOe using a vibrating sample magnetometer (VSM, Lakeshore 7304, USA). The crystal structure of the resulting MMAC was specified employing monochromatized Cu Kα radiation from an X-ray diffractometer (XRD) at 40 mA and 40 kV (λ=1.541874 Å, scanning rate = 3°/min and 2θ range of 10–80 °). The crystalline size diameter (D) and the average size of the as-produced MMAC were determined as per the

Debye-Scherrer and Scherrer equations, respectively. A scanning electron microscope (FESEM, TESCAN MIRA, Czech Republic) was employed to examine the surface morphology of VFB-originated MMAC. At the same time, an Energy Dispersive Spectrometer (INCA X-MAX50, Oxford, UK) was exploited to specify the elemental composition of the said MMAC.

### Adsorption studies of MB and DBT

Firstly, stock solutions of MB dye and DBT (500 mg/L) were prepared by dissolving 0.50 g of MB in 1 L of DW and 1 L of n-hexane, respectively. From these stock solutions, other working solutions were derived. Also, these stock solutions were used to prepare the calibration curves, which were used to determine the pollutant concentration after equilibrium (Figure 1S, supplementary materials). For the adsorption trials of MB dye or DBT, 100 mL of MB solution and 25 mL of DBT solution were separately mixed with a given mass of the as-synthesized MMAC in a round-bottomed flask. The resulting mixtures were shaken at 700 rpm at room temperature (30 °C) until equilibrium was reached. The MMAC-pollutant solutions were centrifuged at 5000 rpm for 5 minutes beyond adsorption to separate the adsorbent particles, while the remaining concentration of each of MB or DBT in their liquid phases was spectrophotometrically determined using a double-beam UV–Vis spectrophotometer (Shimadzu, UV-Visible-160, Japan) at 665 nm for MB and 325 nm for DBT (Hussein and Fadhil, 2021). The results were confirmed by utilizing the mean of two experiments ± SD. The influence of MMAC dosage (0.05–0.50 g), the initial pH of the MB solution (2,4,6,7,8,10), the initial concentration of pollutant (25–200 mg/L), the adsorption temperature (10–60 °C), and the period of adsorption (10–60 min) were optimized to assess their impact on the adsorption capacity ($q_e$, mg/g) and removal efficiency (RE) for both pollutants by MMAC. The pH of MB solutions was optimized by adding 0.1 M HCl or NaOH. The equations used to specify the $q_e$ and RE of both pollutants in their liquid phases are shown in Table 1S (supplementary materials).

### Regeneration trials of the consumed MMAC

The MMAC specimens, exhausted by DBT adsorption, were regenerated and repurposed under typical conditions. In a Soxhlet extraction, n-hexane was used as the solvent to remove DBT from the exhausted MMAC samples. The MMAC specimens were dried at 105 °C for 2h after DBT desorption, and then thermally activated at 500 °C for 30 minutes (Al-Layla et al., 2024). For the desorption of MB from the spent MMAC, a known mass of the exhausted adsorbent was mixed with 25 mL of 0.5 M NaOH, and the mixture was refluxed for 5 h. Later on, the regenerated MMAC was repeatedly rinsed with DW until neutral water was obtained, followed by dehydration at 105 °C for 5 h (Patawat et al., 2020). These procedures were conducted 5 times. The RE of MB or DBT from their liquid phases was tested on the regenerated adsorbent using the optimal experimental parameters established during the investigation.

## RESULTS AND DISCUSSION

### Selection of the best MMAC

The selection of the ideal MMAC was carried out through exploring the influence of the synthesis conditions on the RE of MB dye and DBT from their liquid phases. The effect of the amount of $FeCl_3$ used in the preparation of MMAC on its RE for MB and DBT was evaluated by varying the $FeCl_3$:VFPs impregnation ratio from 1:1 to 3:1, as revealed in Figure 1a.

It was noticed that increasing the $FeCl_3$ amount from 1:1 to 1.5:1 improved the removal efficiency RE of both pollutants. The rise in the RE% for both pollutants resulted from $Fe_2O_3$ and $Fe_3O_4$ particles generated by the breakdown of $FeCl_3$, which can serve as catalysts to gasify neighboring carbon compounds in the parent feed into low-molecular gases, including CO and $CH_4$ (Zhang et al., 2025). Also, the formation of these Fe oxides will increase the number of oxygen vacancies and adsorption sites on the sorbent surface, resulting in better removal of pollutants from their liquid phase (Xu et al., 2020). Nonetheless, when a higher amount of $FeCl_3$ (> 1.5:1 $FeCl_3$:VFPs) was used in the synthesis of the MMAC, the RE% of MB and DBT declined. This outcome may be ascribed to the fact that employing excessive amounts of the activator ($FeCl_3$) may induce crystallization, hence damaging the surface morphology of the resulting sorbents, and
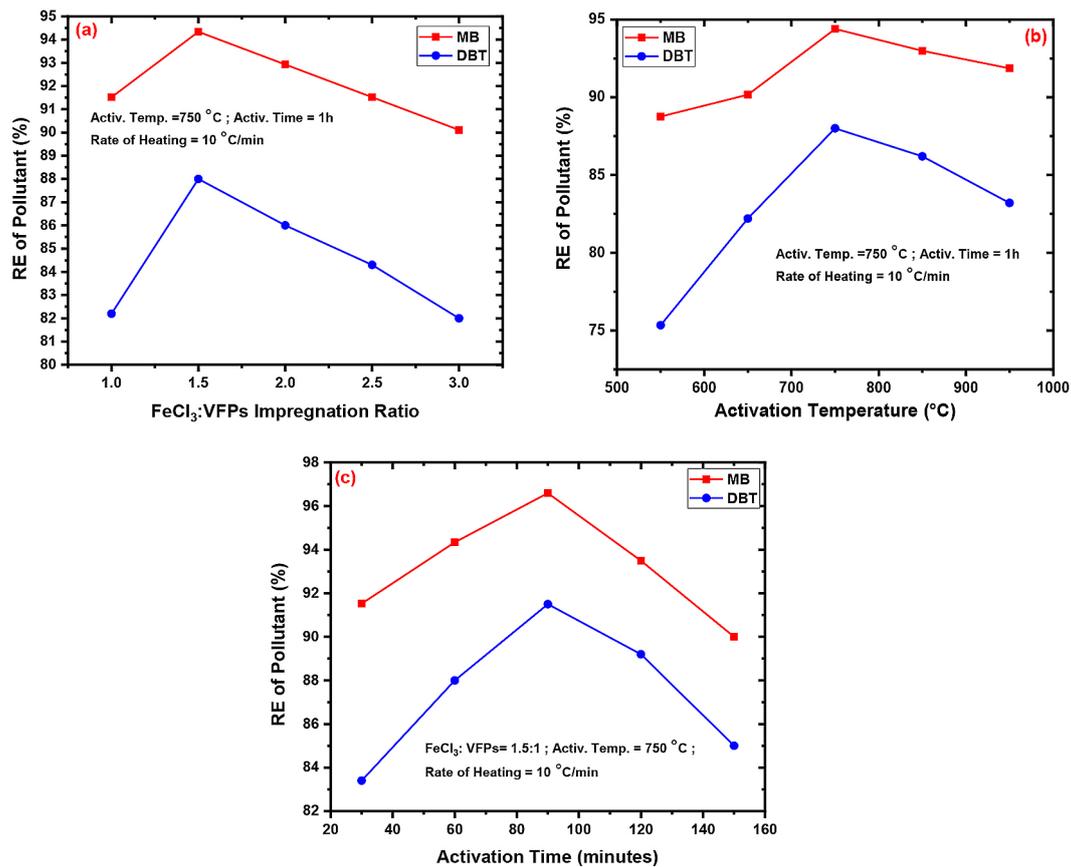
**Figure 1.** Effect of the preparation conditions on the RE % of pollutants from their liquid phases

consequently, the RE% of both MB and DBT diminishes (Xiao et al., 2020).

It can be seen from Figure 1b, which offers the effect of the activation temperature of $FeCl_3$-VFPs mixture at various temperatures in the range of 550 °C to 950 °C using 1.5:1 $FeCl_3$: VFPs, that upon the increment of the activation temperature from 550 °C to 750 °C, the RE% of MB and DBT enhanced. At the lower activation temperatures, there was scant porosity, resulting in only a minor elimination of both contaminants from their liquid phases. As the activation temperature increased, the RE% of MB and DBT increased, particularly at 750 °C. Such findings could be ascribed to the $FeCl_3$ breakdown, which leads to the creation of $Fe_2O_3$ and $Fe_3O_4$ particles, which can act as catalysts to convert carbon ingredients in the authentic VFPs into low-molecular ingredients, like CO and $CH_4$, which in turn increase the surface area of the resulting adsorbent and thus enhance the RE% of the studied pollutants (Xu et al., 2020). Nevertheless, when the activation was conducted at temperatures above 750°C, the RE% of MB and DBT diminished. Such outcomes might be attributed to the potentially powerful sintering effect of

the formed $Fe_2O_3$ and $Fe_3O_4$ particles, which decrease the surface area and O-vacancies, as well as the number of adsorption sites on the resulting MMAC. Also, with an adequate amount of the activator ($FeCl_3$), there is a chance that $Fe_3O_4$ particles will precipitate within the porous structure of the resulting MABC, leading to reduced elimination of MB and DBT from their solutions (Yang et al., 2019). In general, the chemical reaction occurs upon the activation of any carbon precursor using $FeCl_3$ as an activator, and can be summarized as follows (Xu et al., 2020):

Assessing the influence of the activation period on the RE% of MB and DBT from their liquid phases by the resulting adsorbents were accomplished through activating the $FeCl_3$-VFPs at 750 °C from multiple durations ranged from 30–150 minutes, as offered in Figure 3c. It was observed that prolonging the activation time from 30 to 90 minutes resulted in the highest RE% of both pollutants from their liquid media. When the activation period exceeded 90 minutes, the RE% of the contaminants declined. This outcome could be attributed to the softening and sintering of low-volatile chemicals, which result in intermediate melts and clog carbon pores. Also,

the collapse of the porous walls of the micro-meso-porous material caused this change (Xu et al., 2020).

## Identification of the resulting MMAC

The MMAC sample that exhibited superior elimination of both MB and DBT from their liquid phases was identified to explore its texture, morphological, and physicochemical features, as well as its crystallinity. It is evident from Figure 2a, which shows the $N_2$ adsorption-desorption isotherms of $N_2$ gas on the resulting MMAC at 77 K that these samples exhibited type I of adsorption isotherms as per the IUPAC classification, with closed adsorption-desorption cycles, referring to a microporous material (Luo et al., 2022).

The gradual increase in the adsorbed amount of $N_2$ with increasing relative pressure ($P/P_0$) in the range of 0.0–0.40 might be attributed to the saturation of the narrow micropores, implying its microporous structure (Harabi et al., 2024). It was found that the resulting MMAC had $SA_{BET}$ of 1224.80 $m^2/g$. This value is above that established for the MAC prepared from termite feces, which had a $SA_{BET}$ between 250 and 393 $m^2/g$ (Demarchi et al., 2019), and macadamia nut shells, the $SA_{BET}$ of which amounted to 868.0 $m^2/g$ (Harabi et al., 2024). On the other hand, Figure 2b, which shows the pore size distribution of the resulting MMAC, indicates that its pores were primarily distributed in the 1–10 nm size range. Moreover, the curve did not refer to the occurrence of pores that have a size of 100 nm. Additionally, the VFPs-derived MMAC had an average pore diameter of 1.91 nm, signifying its narrow microporous structure. The BJH surface area, which refers to the meso surface area of the adsorbent, was found

to be 189.96 $m^2/g$ with mesopore participation of 15.50, indicating that the texture structure of the VFPs-derived MMAC is microporous with the presence of narrow mesopores.

Exploring the crystalline structure of the resulting VFPs-derived MMAC was carried out using XRD measurements. According to Figure 3, which demonstrates the XRD patterns of the produced magnetic adsorbent, the VFPs-derived adsorbent exhibited a broad peak at $2\theta = 24.10°$, indicating the creation of the amorphous structure of AC. In addition to this peak, other peaks at different positions could be detected in the XRD patterns of the as-created magnetic adsorbent. These bands ensure the formation of the cubic spinals for magnetite ($Fe_3O_4$). The observed diffraction peaks were detected at $2\theta = 33.37$, $2\theta = 35.85°$, $2\theta = 41.05°$, $2\theta = 49.71°$, $2\theta = 54.34°$, and $2\theta = 63.33°$. These diffraction peaks correspond to the (220), (311), (400), (422), (511), and (440) phases, based on the JCPDS file 89–43191 (Siddique et al., 2020). These findings suggest that the formation of a magnetic adsorbent results from the chemical activation of VFPs with $FeCl_3$. Also, the observed diffraction peaks were found in the magnetic AC produced by $FeCl_3$-activation of *Citrus limetta* peels (Siddique et al., 2020). The crystalline size diameter (D) of VFPs-derived magnetic adsorbent was determined, as per the Debye-Scherrer equation. It was found that the values of D ranged from 15.63 to 30.55 nm. On the other hand, the average size of VFPs-derived MMAC, calculated using the Scherer equation, was 27.58 nm. Such results established the nanostructure of the VFPs-derived MMAC.

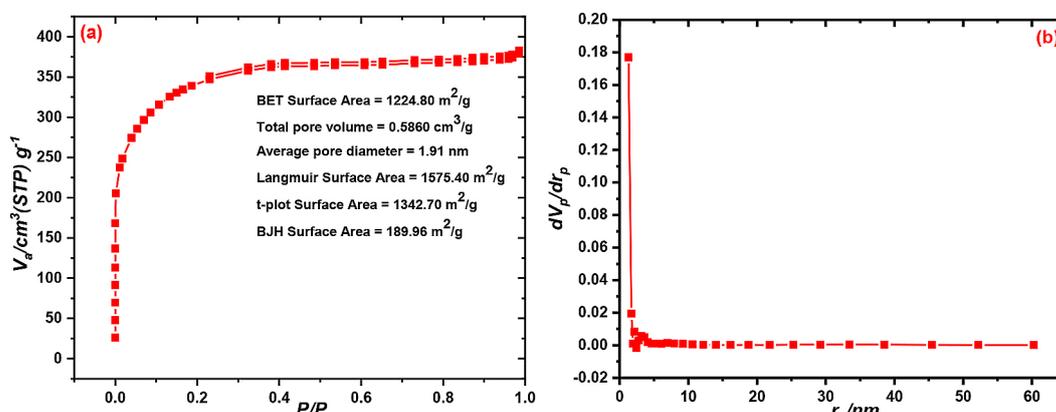The morphology of the VFPs-derived MMAC examined by FESEM at various magnifications



**Figure 2.** The $N_2$ adsorption-desorption isotherms and pore volume distribution of MMAC
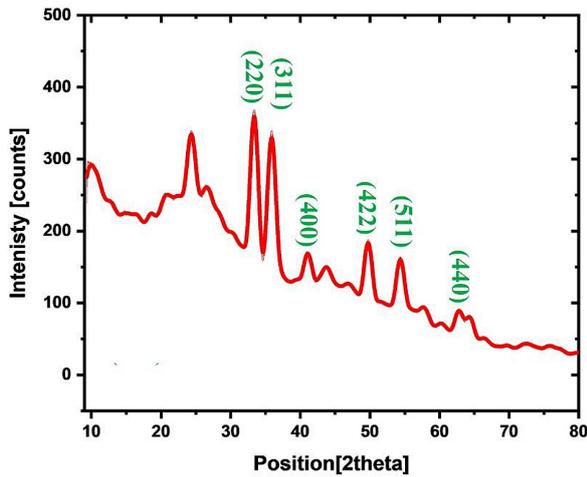
**Figure 3.** The XRD patterns of the resulting MMAC

is illustrated in Figure 4, which shows that the surface of the resulting MMAC is very irregular and entirely covered with voids and hollows, with irregular distribution along the surface. These cracks, voids, and holes are most expected to be

produced as an outcome of the loss of organic volatile materials that occurred through the fast activation of VFPs by $FeCl_3$. Additionally, the surface of the resulting MMAC clearly contained some regularly dispersed crystals, which might represent iron oxide crystals strongly linked to MMAC, as they were not eliminated after washing the resulting adsorbent following $FeCl_3$-activation (Gómez-Avilés et al., 2021). The presence of multiple pores and iron oxide crystals on the surface of the resulting MMAC is compatible with the $SA_{BET}$ and XRD measurements of this MMAC.

The EDX analysis was performed to determine the elemental composition of the VFPs-derived MMAC. It is apparent from Figure 5, which shows the EDX mapping of the produced MMAC, that C (76.76%), O (20.44%), and Fe (2.79%) were the main elements forming this adsorbent. The minor percentage of Fe and the absence of Cl in the elemental analysis mapping of the as-created MMAC confirmed that most of the
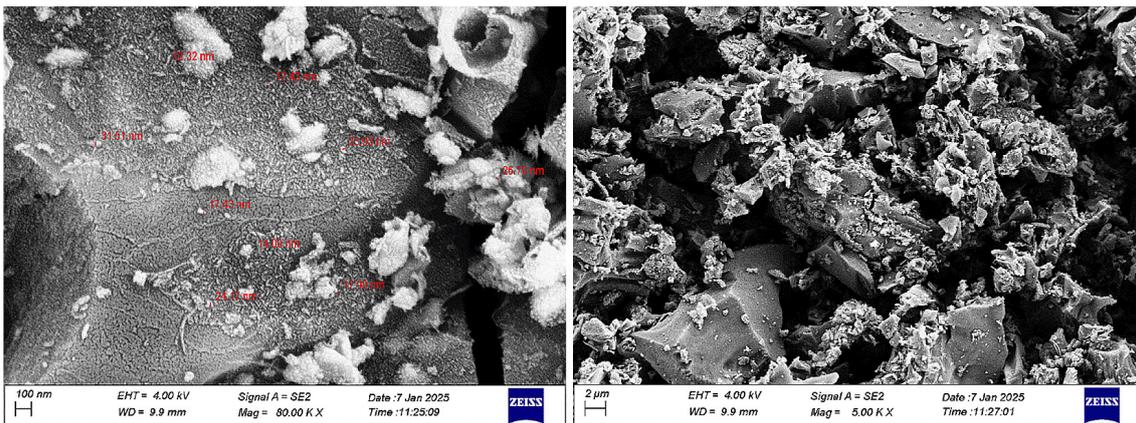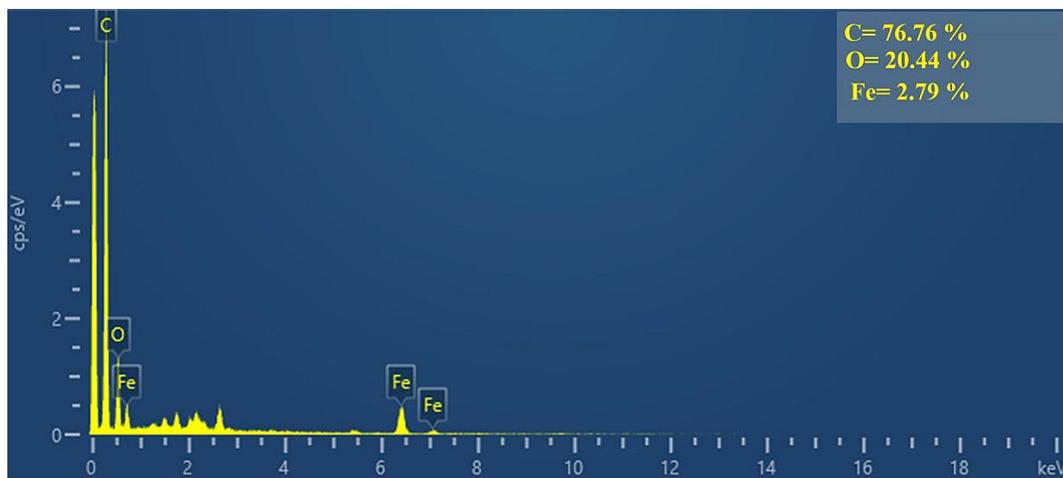


**Figure 4.** FESEM images of the resulting MMAC



**Figure 5.** EDX mapping of the resulting MMAC

activator was consumed upon the transformation of VFPs into MMAC. Also, the presence of Fe and O confirms that iron oxides were present in the resulting adsorbent, which is consistent with the XRD measurements. Moreover, the presence of iron oxides will increase the number of active sites, which aid in the elimination of pollutants from the solution.

The magnetic features of the as-created MMAC were examined by VSM measurements (Figure 6). The typical MMAC exhibited a saturation magnetization of 0.085 emu/g. This magnetic response was due to the involvement of $Fe_3O_4$ in the carbon skeleton of the resulting MMAC, as proven by the XRD patterns of the prepared MMAC. However, the minor saturation magnetization of the produced MMAC is attributable to the low Fe content in the elemental analysis mapping of the prepared adsorbent, as detected by EDX.

## Optimization of MB and DBT adsorption by the resulting MABC

The removal of MB dye from the aqueous phase and DBT from the model oil was evaluated by optimizing the variables affecting the adsorption of the studied pollutants from their respective liquid phases. The impact of the pH on the RE % of MB from its liquid phase by the resultant MMAC is exposed in Figure 7.

It was observed that when the initial pH of the solution climbed from 2 to 9, the RE% of MB increased. At a pH of 9.0, the RE% of MB from its aqueous phase by the resultant MMAC reached its maximum. This outcome suggests that the

adsorbate molecules undergo a structural change when the solution pH is altered, due to dispersion forces and electrostatic interactions, the two main forces promoting contact between the adsorbent and MMAC. MB is a cationic dye with a positively charged quaternary ammonium group ($=N^+(CH_3)_2Cl^-$), as is widely known. The ($O-H$) functional groups on MMAC are protonated in acidic environments into ($-OH^{2+}$) groups. The ($O-H$) functional groups on MMAC are protonated in acidic environments into ($-OH^{2+}$), which creates electrostatic repulsion between the species of MB and the surface groups of the adsorbent, which in turn lowers the RE% of MB (Dalmaz and Özak, 2024). The competition for $H^+$ significantly decreases as the pH rises towards alkaline conditions, and the ($O-H$) groups on the MMAC surface deprotonate to produce $-O^-$, increasing the electrostatic attraction between the MMAC and MB molecules. Consequently, the RE% of MB enhances (Dalmaz and Özak, 2024). The obtained results are similar to those reported in the literature for MB adsorption by several adsorbents (Dalmaz and Özak, 2024; Azoulay et al., 2020).

The impact of the MMAC dose was examined by adding (0.05–0.40 g) of MMAC into 100 mL of a 200 mg/L MB solution and 25 mL of a 200 mg/L DBT solution. The experiments were conducted under the conditions revealed in Figure 8. The results showed that as the amount of MMAC increases, the RE% of both pollutants from their liquid phases increases significantly. Adsorption of MB and DBT by the MMAC increases rapidly at first, but then the rate of growth slows. This is because the number of active sites for adsorbing
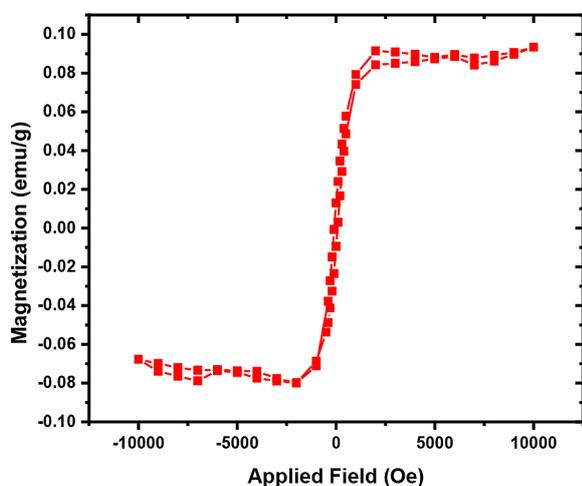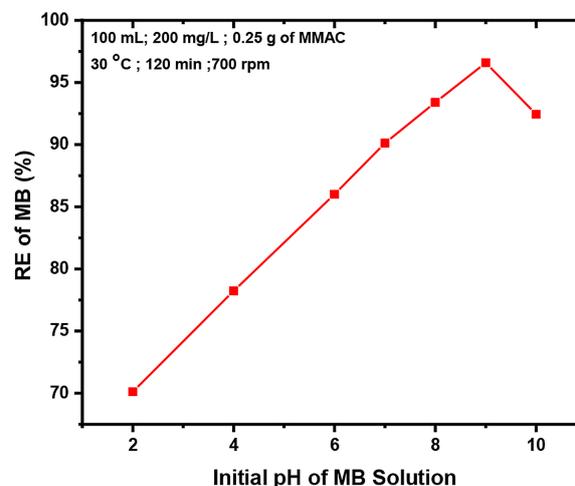
**Figure 6.** The VSM curves of the resulting MMAC

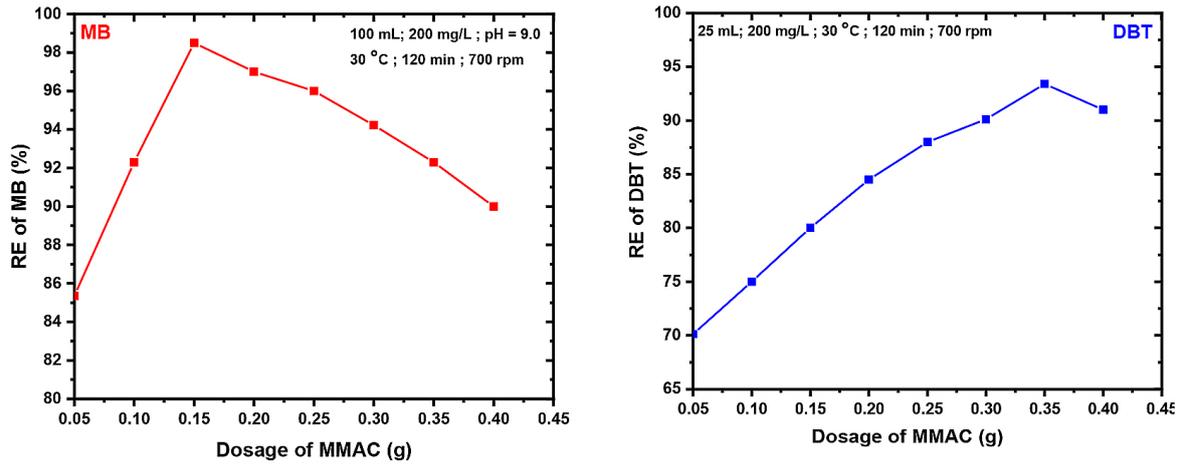**Figure 7.** Effect of pH on the RE% of MB by the resulting MMAC

**Figure 8.** Effect of MMAC dosage on the RE% of MB and DBT from their liquid phases

the adsorbate species increases with an increment in MMAC dose. Also, with the increase in MMAC mass, the adsorbate molecules in the solution will outnumber the adsorbent particles, leading to a decrease in their accessibility to the adsorbent surface (Saeed et al., 2024). However, the highest RE% for MB was achieved with 0.15 g of MMAC, compared to 0.35 g, which yielded the maximum elimination of DBT from the model. Nonetheless, a drop in the RE% of both pollutants from their solutions was noticed when the MMAC mass exceeded the typical dosage. This was due to a decrease in the overall surface area resulting from the aggregation of large masses of MMAC particles. Consequently, this will reduce the RE% for both contaminants. The observed findings were in line with those reported by other researchers upon the RE of MB and DBT from their solutions by various adsorbents (Saeed et al., 2024;

Hussein and Fadhil, 2021; Al-Layla et al., 2024; Dalmaz and Özak, 2024; Azoulay et al., 2020).

One of the most important factors influencing adsorption investigation is the adsorption temperature. Therefore, assessing the influence of this parameter was achieved by examining the adsorption of MB and DBT at multiple temperatures (10–60 °C), while keeping other variables unchanged, as exposed in Figure 9.

This figure illustrates that the RE% of MB and DBT increased as the adsorption temperature rose from 10 °C to 30 °C, indicating the endothermic nature of the adsorption process. Collisions between the MMAC particles and the adsorbate species increase along with temperature, thereby improving the RE%. Nonetheless, as the temperature exceeded the ideal ones, the RE% of MB and DBT dropped, as a consequence of the weakening of the attraction forces between the MMAC surface and the adsorbate molecules, causing a
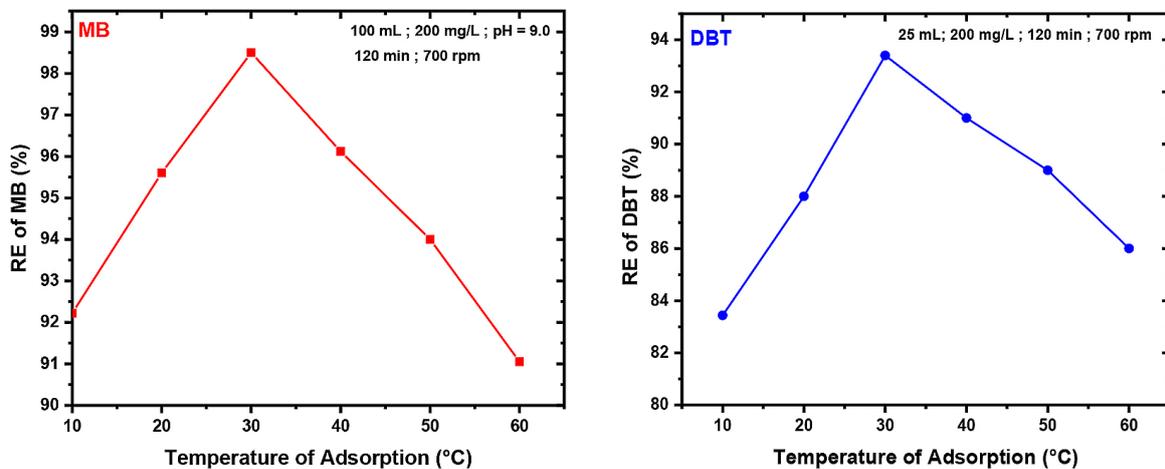


**Figure 9.** Effect of the adsorption temperature on the RE% of MB and DBT from their liquid phases

decline in the RE % (Dalmaz and Özak, 2024; Saeed et al., 2024). Similar outcomes were reported by several authors during the adsorption of MB or DBT from their liquid phases (Saeed et al., 2024; Dalmaz and Özak, 2024).

Figure 10 shows the results of investigating the impact of contact time on the RE% of MB dye from wastewater and DBT from model oil at various durations, ranging from 10 to 120 minutes, under the conditions shown in the legend of this figure. It was observed that the longer the contact period, the greater the contaminant adsorption. In the first 10 minutes of the adsorption process, the adsorption of both pollutants from their liquid phases was fast, so that RE% reached 90% for MB dye and 92% for DBT. Afterwards, the increment of the RE % of the contaminants was slow. Such findings could be attributed to the availability of numerous active surface sites on MMAC during the initial stage of the adsorption process (Mani et al., 2023). Over time,

the number of these effective positions declines, and the adsorption process slows. Once equilibrium is attained, there is no further rise in the RE %. Equilibrium was achieved after 60 minutes for MB dye and 40 minutes for DBT.

The initial concentration effect of each contaminant on its RE% by the said MMAC was examined in the range of 25–200 mg/L, applying the conditions provided in the legend of Figure 11. The findings unequivocally showed that when the initial concentration of the pollutant rises, the RE% declines. At the low initial contaminant concentration, the MMAC surface may have a significant number of vacant active sites, which could explain this phenomenon (Saeed et al., 2024; Zakaria et al., 2021). On the other hand, the presence of a high concentration of the pollutant restricted the number of free active sites at high initial dye concentrations, leading to a drop in the RE % (Hussein and Fadhil, 2021; Zakaria et al.,
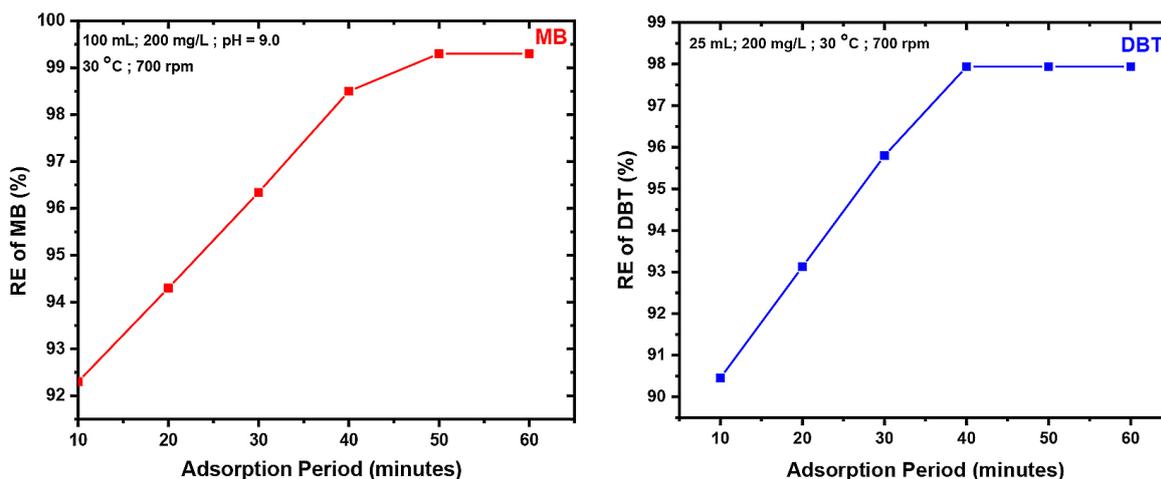


**Figure 10.** Effect of the adsorption period on the RE% of MB and DBT from their liquid phases
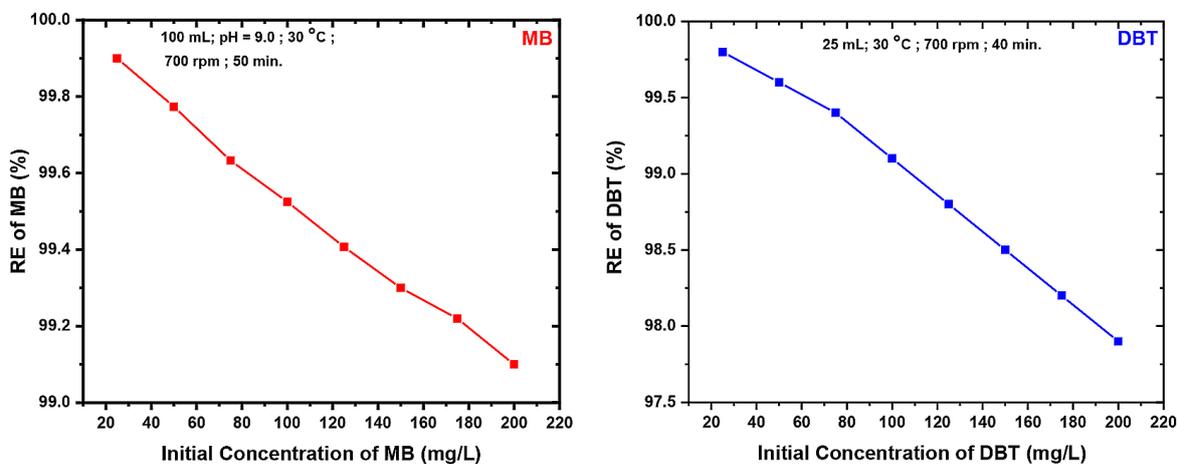


**Figure 11.** Effect of the pollutant's initial concentration on its RE% by MMAC

2021). Similar observations were established by many authors during the adsorption of MB from wastewater and DBT from model oils using various adsorbents (Saeed et al., 2024; Hussein and Fadhil, 2021; Zakaria et al., 2021).

**Isothermal studies of pollutant adsorption by MMAC**

The isotherm study is essential for a comprehensive understanding of solid-liquid adsorption. It is crucial to comprehend the amount of adsorbate retained by the adsorbent and the concentration of adsorbate remaining in the solution once equilibrium adsorption is attained (Maiti et al., 2023). This study examined the Langmuir, Freundlich, and Temkin isotherm models to analyze the pollutant adsorption mechanism, the behavior of the adsorbent, and the favorability of the process on the MMAC surface (Maiti et al., 2023).

The non-linear forms of these isotherms, which are illustrated in Table 2S (supplementary material) were applied to analyze the adsorption data of MB and DBT from the liquid phase, while the non-linear plots of MB and DBT adsorption

are offered in Figure 12. On the basis of the outcomes deduced from these isotherms, the $R_L$ values for MB and DBT adsorption over MMAC suggested that the adsorption of these pollutants from their liquid phases was favorable, as $0 < R_L < 1$ (Saeed et al., 2024). Moreover, the values of n for the adsorption of contaminants by the resulting MMAC were above 1.0, indicating that the adsorption of MB and DBT by the newly created MMAC is preferable. On the basis of the adsorption data for MB and DBT by the MMAC shown in Table 1, the goodness of fit to the experimental database is ranked as follows: Langmuir, Freundlich, and Temkin. This conclusion was reached based on the $R^2$ value of the Langmuir fitting findings, which surpassed that of the Freundlich and Temkin models, indicating that the Langmuir model more accurately characterizes the adsorption isotherm effect than the Freundlich and Temkin isotherms, with adsorption primarily governed by monolayer adsorption on a homogeneous surface (Zheng et al., 2021).The maximum adsorption capacity ($Q_{max}$, mg/g) derived from the Langmuir isotherm for MB and DBT from their

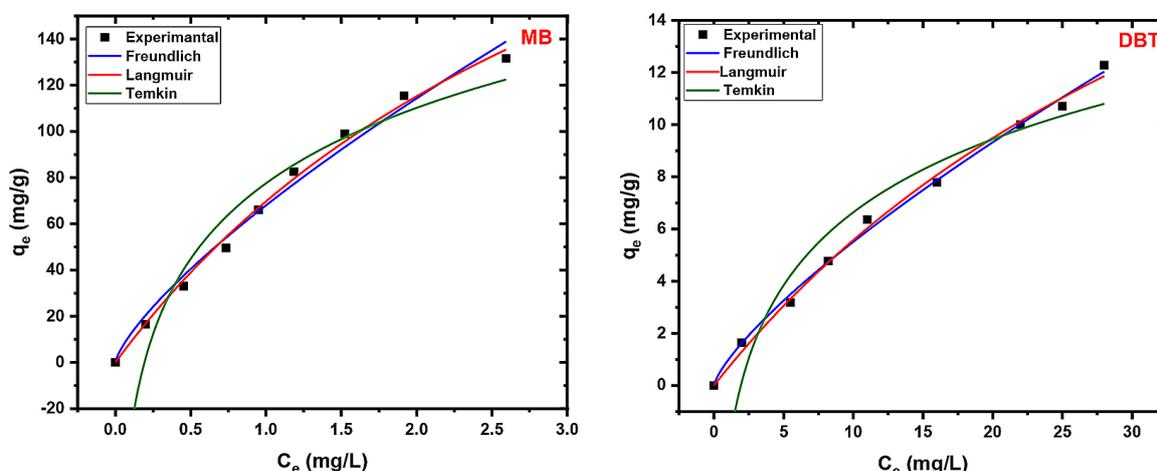**Figure 12.** The non-linear adsorption isotherms of the pollutants over the resulting MMAC

**Table 1.** Values for the adsorption isotherms used for analyzing MB and DBT adsorption by MMAC

| MB | | | | | | | | | |
|---|---|---|---|---|---|---|---|---|---|
| Langmuir | | | | Freundlich | | | Temkin | | |
| $R^2$ | $q_m$ (mg/g) | $K_L$ | $R_L$ | $R^2$ | n (mg/g) | $K_F$ | $R^2$ | A | B |
| 0.9955 | 331.50 | 0.2662 | 0.0185 | 0.9831 | 1.35 | 68.00 | 0.9579 | 5.18 | 47.12 |
| DBT | | | | | | | | | |
| Langmuir | | | | Freundlich | | | Temkin | | |
| $R^2$ | $q_m$ (mg/g) | $K_L$ | $R_L$ | $R^2$ | n (mg/g) | $K_F$ | $R^2$ | A | B |
| 0.9956 | 31.83 | 0.0212 | 0.1908 | 0.9901 | 1.33 | 0.9589 | 0.9454 | 0.51 | 4.04 |

solutions by MMAC were found to be 331.50 mg/g and 31.83 mg/g, respectively.

In comparison with $Q_{max}$ for the same adsorbates over multiple adsorbents in the literature (Table 4S, supplementary material), the MMAC prepared from VFPs exhibited superior values of $Q_{max}$ for MB and DBT than those established for some adsorbents offered in Table 4S (supplementary material), indicating the effectiveness of the as-synthesized MMAC in eliminating various pollutants from various liquid phases with a high adsorption capacity (Yaseen et al., 2021; Saleh and Danmaliki, 2016; Dalmaz and Sivrikaya Özak, 2024; Patawat et al., 2020; Moradi et al., 2018). The elevated adsorption capacity of the adsorbent prepared here, compared with those prepared by other authors, could be attributed to its higher surface area and the active sites on its surface, which are believed to play a vital role in the adsorption process.

## Kinetics studies of MB and DBT adsorption by MMAC

The kinetic data of MB and DBT adsorption by VFPs-derived MMAC were examined using three popular kinetic models: the pseudo-1st-order (PFO), pseudo-2nd-order (PSO), and intra-particle diffusion (IPD). The non-linear equations of these kinetic models were applied to express the adsorption of MB and DBT by the VFPs-derived MMAC.

Table 2 lists the values of the constant kinetic parameters, while Figure 13 displays the results of fitting the non-linear kinetic model to the experimental data. Table 2 shows that PSO was more accurate in describing the adsorption behavior of MB and DBT from their liquid phases than PFO. This conclusion was adopted based on the $R^2$ value. The $R^2$ values for MB and DBT adsorption on the VFPs-derived MMAC were much greater than those for PFO. PSO also showed a strong agreement with experimental data, with a $q_e$ value near that empirically estimated compared with PFO (Saeed et al., 2024; Hussein and Fadhil, 2021). Thus, it can be concluded that the PSO kinetic model is more effective than the PFO model in characterizing MB and DBT adsorption by MMAC (Patawat et al., 2020). These results correspond with those documented by Saeed et al.(2024) and Jawad et al. (2019)during the adsorption of DBT and MB from their solutions using various adsorbents. Additionally, the
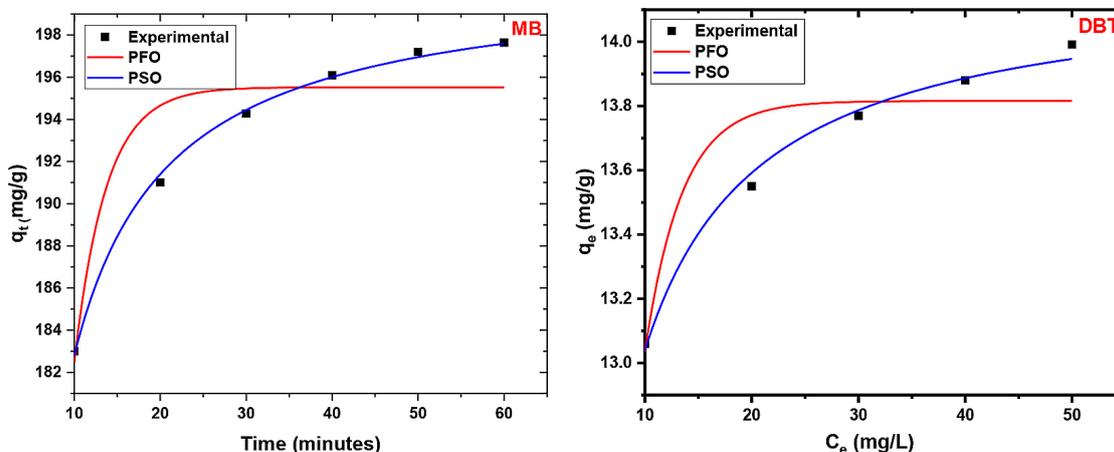


**Figure 13.** The non-linear adsorption kinetics models of the pollutants over the resulting MMAC

**Table 2.** Values for the adsorption isotherms used for analyzing MB and DBT adsorption by MMAC

| MB | | | | | | | | |
|---|---|---|---|---|---|---|---|---|
| PFO | | | PSO | | | IPD | | |
| $R^2$ | $q_t$ (mg/g) | $k_1$ (L/mg) | $R^2$ | $q_t$ (mg/g) | $k_2$ (L/mg) | $R^2$ | $K_{diff}$ | C |
| 0.8529 | 195.52 | 0.2708 | 0.9980 | 200.84 | 0.0050 | 0.71949 | 23.35 | 51.30 |
| DBT | | | | | | | | |
| PFO | | | PSO | | | IPD | | |
| $R^2$ | $q_t$ (mg/g) | $k_1$ (L/mg) | $R^2$ | $q_t$ (mg/g) | $k_1$ (L/mg) | $R^2$ | $K_{diff}$ | C |
| 0.8402 | 12.82 | 0.2879 | 0.9917 | 14.19 | 0.0795 | 0.7623 | 1.90 | 2.97 |

experimental adsorption data for MB and DBT over the VFPs-derived MMAC were examined using Weber's IPD model (Figure 2S, supplementary material). The mechanisms and rate-limiting phases influencing the adsorption kinetics of pollutants can be estimated using this model. As it was shown in Figure 13, the regression line did not pass through the origin. This means that this model cannot fully show the rate-limiting step of MB and DBT adsorption by the resultant MMAC (Hussein and Fadhil, 2021; Jawad et al., 2019).

### The RE of MB and DBT from their real samples

The current study further investigated the RE of actual gasoline using the as-developed MMAC under the previously obtained typical experimental conditions. Under these conditions, 62.22% of the S-containing compounds could be eliminated from the commercial petrol sample. This result was insufficient compared to the model fuel. This is because the commercial petrol sample contains

more complex isomers of DBT, such as 2-MDBT, 2,4,6-Tri-DMDBT, 4-MDBT, 2,4-DMDBT, and 4,6-DMDBT, which are more challenging to eliminate than DBT, as an outcome of the steric hindrance induced by their side alkyl moieties, resulting in a lower RE% (Yaseen et al., 2021; Saeed et al., 2024). This finding was also established by other researchers upon the desulfurization of real gasoline samples using various adsorbents (Yaseen et al., 2021; Saeed et al., 2024).

Also, the RE% of MB in their solutions in river water and well water (WW) was evaluated by applying the ideal experimental conditions obtained earlier. As per Figure 14, the RE% of MB from its solutions in RW and WW were below that obtained with its solution in DW. This result was anticipated, as DW is purified water and contains no dissolved contaminants (ions and salts), which could potentially compete with the ability of MMAC to adsorb the MB species. It was also observed that the RE% of MB from RW was higher than that of WW. These consequences may be attributed to the increased concentrations of dissolved salts and ions in WW compared to RW, leading to more effective elimination of MB.
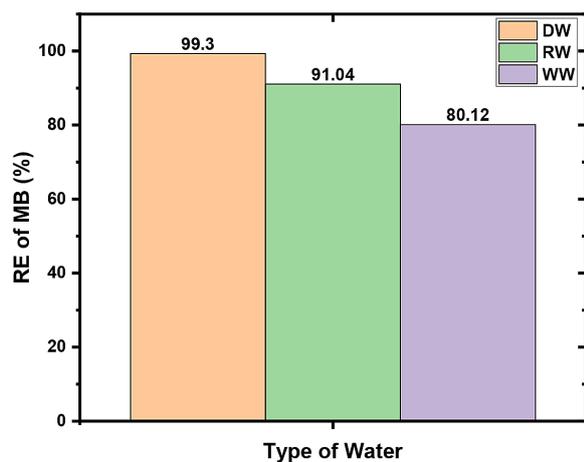
### Desorption trials of the studied pollutants

The FESEM images of the MMAC exhausted as an outcome of the adsorption of MB or DBT are depicted in Figure 15.

These images demonstrated that the MMAC surface, after adsorbing MB or DBT, was smooth, although some pores were present. Also, many crystals were visible on its surface, representing adsorbed MB or DBT species. Another clue to the exhaustion of the MMAC surface by the MB or
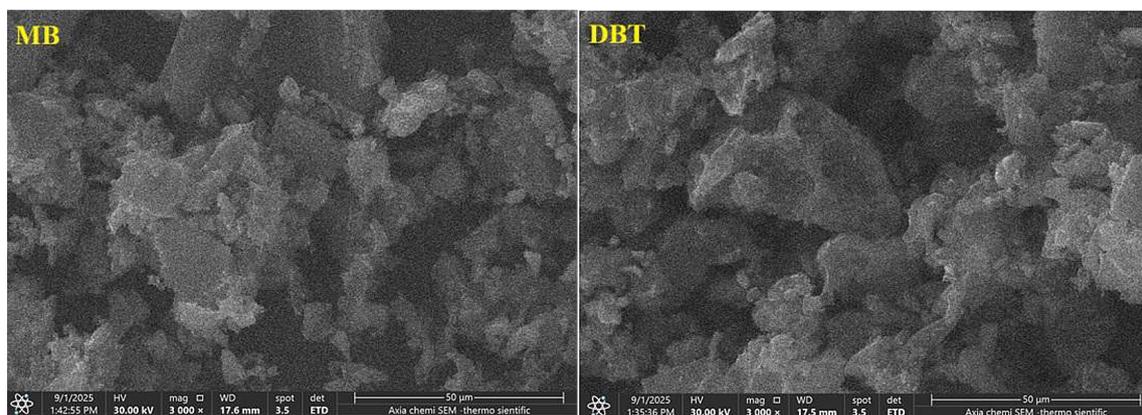


**Figure 14.** Effect of type of water on the RE% of MB



**Figure 15.** FESEM images of MMAC after the adsorption of MB and DBT on its surface

**Table 3.** Elemental analysis outcomes after the adsorption of MB or DBT on the MMAC surface

| Before adsorption | | | | |
|---|---|---|---|---|
| C% | O% | Fe% | N% | S% |
| 76.76 | 20.44 | 2.79 | - | - |
| After MB adsorption | | | | |
| C% | O% | Fe% | N% | S% |
| 59.30 | 25.20 | 2.70 | 11.80 | 0.90 |
| After DBT adsorption | | | | |
| C% | O% | Fe% | N% | S% |
| 67.9 | 24.30 | 7.0 | - | 0.80 |

DBT molecules is the EDX analysis, with the elemental analysis outcomes provided in Table 3.

The findings in the above table showed that, besides C, O, Fe, N, and S could be detected in the EDX mapping of the spent adsorbent, confirming the adsorption of MB or DBT on the MMAC surface. To recover the adsorptive efficiency of the spent MMAC, MB, or DBT adsorbed on MMAC, MB or DBT adsorbed on the exhausted adsorbent were stripped, as previously illustrated. After each run of the desorption trials, the regenerated MMAC was applied to the RE of MB or DBT from its liquid phase, using the previously established adsorption settings.

Figure 16 showed that the regenerated MMAC could strip MB or DBT from its liquid phase even after the 4th regeneration run, with reasonable efficacy. The continual decline in the RE% of the studied pollutants by the regenerated MMAC could be attributed to factors, such as the gradual degradation of the adsorbent material with repeated usage and treatment at high pH levels, besides the saturation of active sites by the contaminant species, leading to a decrease in the number of the active positions for adsorbing more molecules of the contaminant. The observed findings were compatible with those established by other authors (Saeed et al., 2024; Hussein and Fadhil, 2021; Jawad et al., 2019).

## Suggested mechanisms for pollutants removal by MMAC

The attachment of the adsorbate species to the surface of any adsorbent can occur through physical contact forces (van der Waals forces or electrostatic) or through chemical interaction (chemisorption) (Al-Layla et al., 2024). It was established that pore filling is the primary mechanism by which any given adsorbent eliminates
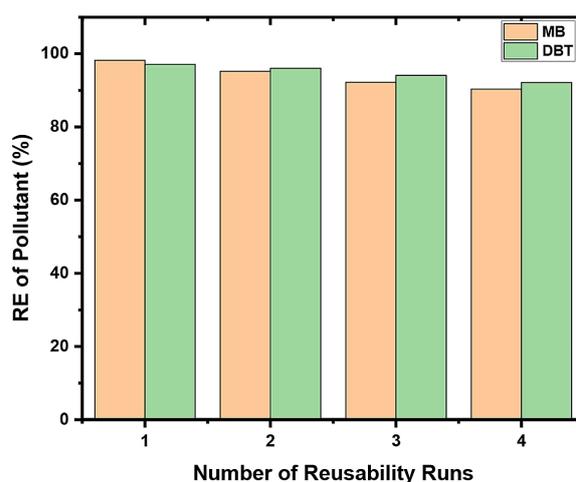


**Figure 16.** Effect of the reusability runs on the RE% of MB and DBT

pollutants. In addition to this mechanism, several auxiliary mechanisms contribute to the attachment of adsorbate species to the adsorbent surface, including acid-base interactions and the adsorption on active sites. For the adsorption of DBT and MB, π-π complexation is the mechanism most commonly proposed for the exclusion of thiophene derivatives by AC, alongside other mechanisms (Yassen et al., 2021; Hussein and Fadhil, 2021). Also, the M-S interactions are believed to contribute to the elimination of S-species from the model oil (Al-Layla et al., 2024).

## CONCLUSIONS

The MMAC prepared via FeCl$_3$-activation of VFPs in a one-step process had a BET surface area of 1224.80 m$^2$/g and a mean pore diameter of 1.91 nm, demonstrating its microporous structure. This adsorbent successfully eliminated MB dye from its liquid phase and DBT from model

oil. The elimination of 200 mg/L MB dye from its solution reached 99.30% using 0.15 g of the MMAC at 30 °C for 50 minutes and a pH of 9.0, while the highest removal of DBT from the model (200 mg/L) was to 97.93% using 0.35 g of the MMAC at 30 °C for 40 minutes. The adsorption of MB dye and DBT from their liquid phases followed the Langmuir isotherm and the pseudo-2nd-order kinetic model. At the typical working variables, the maximum adsorptive capacity for MB was 331.50 mg/g compared with 31.83 mg/g for DBT. Additionally, at the optimal working settings, desulfurization of real oil fuel reached 62.22%. At the same time, the elimination of MB from its solutions in river and well waters amounted to 91.04% and 80.12%, respectively. Moreover, under optimal conditions, the reusability of the studied pollutants on the regenerated adsorbent achieved elimination performance for both contaminants above 90% in the 4th cycle. In conclusion, using agricultural solid waste to prepare eco-friendly novel adsorbents promotes sustainability and effective waste management.

## Acknowledgements

## REFERENCES

1. Ahmed, M. J. (2011). Preparation of activated carbons from date stones by chemical activation method using $FeCl_3$ and $ZnCl_2$ as activating agents. *Journal of Engineering*, *17*(4).

2. Al-Layla, N. M. T., Yahya, O. M., Altamer, M. H., Fadhil, A. B. (2024). Kinetic and isothermal investigation on the excellent adsorption removal of dibenzothiophene from model fuel over MnO/activated carbon composite. *Russian Journal of General Chemistry*, *94*(4), 922–934. https://doi.org/10.1134/S1070363224040200

3. Azoulay, K., Bencheikh, I., Moufti, A., Dahchour, A., Mabrouki, J., El Hajjaji, S. (2020). Comparative study between static and dynamic adsorption efficiency of dyes by the mixture of palm waste using the central composite design. *Chemical Data Collections*, *27*, 100385. https://doi.org/10.1016/j.cdc.2020.100385

4. Cheruiyot, G. K., Wanyonyi, W. C., Kiplimo, J. J., Maina, E. N. (2019). Adsorption of toxic crystal violet dye using coffee husks: Equilibrium, kinetics and thermodynamics study. *Scientific African*, *5*, e00116. https://doi.org/10.1016/j.sciaf.2019.e00116

5. Dalmaz, A., Sivrikaya Özak, S. (2024). Methylene blue dye efficient removal using activated carbon developed from waste cigarette butts: Adsorption, thermodynamic and kinetics. *Fuel*, *372*, 132151. https://doi.org/10.1016/j.fuel.2024.132151

6. Danish, M., Ahmad, T., Hashim, R., Said, N., Akhtar, M. N., Mohamad-Saleh, J., Sulaiman, O. (2018). Comparison of surface properties of wood biomass activated carbons and their application against rhodamine B and methylene blue dye. *Surfaces and Interfaces*, *11*, 1–13. https://doi.org/10.1016/j.surfin.2018.02.001

7. Danmaliki, G. I., Saleh, T. A. (2017). Effects of bimetallic Ce/Fe nanoparticles on the desulfurization of thiophenes using activated carbon. *Chemical Engineering Journal*, *307*, 914–927. https://doi.org/10.1016/j.cej.2016.08.143

8. Dayana Priyadharshini, S., Manikandan, S., Kiruthiga, R., Rednam, U., Babu, P. S., Subbaiya, R., Karmegam, N., Kim, W., Govarthanan, M. (2022). Graphene oxide-based nanomaterials for the treatment of pollutants in the aquatic environment: Recent trends and perspectives – A review. *Environmental Pollution*, *306*, 119377. https://doi.org/10.1016/j.envpol.2022.119377

9. Demarchi, C. A., Michel, B. S., Nedelko, N., Ślawska-Waniewska, A., Dłużewski, P., Kaleta, A., Minikayev, R., Strachowski, T., Lipińska, L., Dal Magro, J., Rodrigues, C. A. (2019). Preparation, characterization, and application of magnetic activated carbon from termite feces for the adsorption of Cr(VI) from aqueous solutions. *Powder Technology*, *354*, 432–441. https://doi.org/10.1016/j.powtec.2019.06.020

10. Djilani, C., Zaghdoudi, R., Djazi, F., Bouchekima, B., Lallam, A., Magri, P. (2016). Preparation and characterisation of activated carbon from animal bones and its application for removal of organic micropollutants from aqueous solution. *Desalination and Water Treatment*, *57*(52), 25070–25079. https://doi.org/10.1080/19443994.2016.1151379

11. Fayazi, M., Taher, M. A., Afzali, D., Mostafavi, A. (2015). Removal of dibenzothiophene using activated carbon/γ-$Fe_2O_3$ nano-composite: kinetic and thermodynamic investigation of the removal process. *Analytical and Bioanalytical Chemistry Research*, *2*(2), 73–84.

12. Gómez-Avilés, A., Peñas-Garzón, M., Belver, C., Rodriguez, J. J., Bedia, J. (2021). Equilibrium, kinetics and breakthrough curves of acetaminophen adsorption onto activated carbons from microwave-assisted $FeCl_3$-activation of lignin. *Separation and Purification Technology*, *278*, 119654. https://doi.

org/10.1016/j.seppur.2021.119654

13. Harabi, S., Guiza, S., Álvarez-Montero, A., Gómez-Avilés, A., Belver, C., Rodríguez, J. J., Bedia, J. (2024). Adsorption of 2,4-dichlorophenoxyacetic acid on activated carbons from macadamia nut shells. *Environmental Research*, *247*, 118281. https://doi.org/10.1016/j.envres.2024.118281

14. Hussein, A. A., Fadhil, A. B. (2021). Kinetics and isothermal evaluations of adsorptive desulfurization of dibenzothiophene over mixed bio-wastes derived activated carbon. *Energy Sources, Part A: Recovery, Utilization and Environmental Effects*, *0*(0), 1–20. https://doi.org/10.1080/15567036.2021.1895372

15. Jawad, A. H., Razuan, R., Appaturi, J. N., Wilson, L. D. (2019). Adsorption and mechanism study for methylene blue dye removal with carbonized watermelon (*Citrullus lanatus*) rind prepared via one-step liquid phase $H_2SO_4$ activation. *Surfaces and Interfaces*, *16*, 76–84. https://doi.org/10.1016/j.surfin.2019.04.012

16. Julinawati, J., Rahmi, R., Karnain, Z. P., Mustafa, I., MZ, K., Farida, M., Kacaribu, A. A. (2025). Preparation of magnetic-activated biocarbon composite from Red Algae for dye removal from water. *Journal of Ecological Engineering*, *26*(8), 67–85. https://doi.org/10.12911/22998993/203746

17. Luo, Y., Zeng, L., Zhao, Y., Zhao, Z., Wei, M., Jiang, B., Fan, J., Li, D. (2022). Roles of $ZnCl_2$ and $FeCl_3$ in preparing high performance corn stover-based carbon materials for efficient removal of Cr (VI) from wastewater. *Journal of Water Process Engineering*, *47*, 102743. https://doi.org/10.1016/j.jwpe.2022.102743

18. Maiti, P., Siddiqi, H., Kumari, U., Chatterjee, A., Meikap, B. C. (2023). Adsorptive remediation of azo dye contaminated wastewater by ZnCl2 modified bio-adsorbent: Batch study and life cycle assessment. *Powder Technology*, *415*, 118153. https://doi.org/10.1016/j.powtec.2022.118153

19. Mani, D., Elango, D., Priyadharsan, A., Al-Humaid, L. A., Al- Dahmash, N. D., Ragupathy, S., Jayanthi, P., Ahn, Y.-H. (2023). Groundnut shell chemically treated with KOH to prepare inexpensive activated carbon: Methylene blue adsorption and equilibrium isotherm studies. *Environmental Research*, *231*, 116026. https://doi.org/10.1016/j.envres.2023.116026

20. Moradi, M., Karimzadeh, R., Moosavi, E. S. (2018). Modified and ion exchanged clinoptilolite for the adsorptive removal of sulfur compounds in a model fuel: New adsorbents for desulfurization. *Fuel*, *217*, 467–477. https://doi.org/10.1016/j.fuel.2017.12.095

21. Oliveira, L. C., Pereira, E., Guimaraes, I. R., Vallone, A., Pereira, M., Mesquita, J. P., Sapag, K. (2009). Preparation of activated carbons from coffee husks utilizing $FeCl_3$ and $ZnCl_2$ as activating agents. *Journal of Hazardous Materials*, *165*(1–3), 87–94.

22. Patawat, C., Silakate, K., Chuan-Udom, S., Supanchaiyamat, N., Hunt, A. J., Ngernyen, Y. (2020a). Preparation of activated carbon from *Dipterocarpus alatus* fruit and its application for methylene blue adsorption. *RSC Advances*, *10*(36), 21082–21091. https://doi.org/10.1039/D0RA03427D

23. Patawat, C., Silakate, K., Chuan-Udom, S., Supanchaiyamat, N., Hunt, A. J., Ngernyen, Y. (2020b). Preparation of activated carbon from *Dipterocarpus alatus* fruit and its application for methylene blue adsorption. *RSC Advances*, *10*(36), 21082–21091. https://doi.org/10.1039/D0RA03427D

24. Pathania, D., Sharma, S., Singh, P. (2017). Removal of methylene blue by adsorption onto activated carbon developed from Ficus carica bast. *Arabian Journal of Chemistry*, *10*, S1445–S1451. https://doi.org/10.1016/j.arabjc.2013.04.021

25. Razmi, F. A., Mohamed Noor, M. H., Ngadi, N. (2025). Adsorptive desulfurization performance hierarchical magnetic biochar from leaf litter for dibenzothiophene of diesel and tire pyrolysis oil. *Journal of Molecular Liquids*, *436*, 128292. https://doi.org/10.1016/j.molliq.2025.128292

26. Rekos, K., Kampouraki, Z.-C., Panou, C., Baspanelou, A., Triantafyllidis, K., Deliyanni, E. (2021). Adsorption of DBT and 4,6-DMDBTon nanoporous activated carbons: the role of surface chemistry and the solvent. *Environmental Science and Pollution Research*, *28*(42), 59050–59062. https://doi.org/10.1007/s11356-020-08242-0

27. Saeed, H. N., Fadhil, A. B., Shareef, O. A. (2024). Isothermal and kinetics investigation of dibenzothiophene removal from model fuel by activated carbon developed from mixed date seed and PET wastes. *Journal of Ecological Engineering*, *25*(3), 38–52. https://doi.org/10.12911/22998993/177628

28. Saleh, T. A., Danmaliki, G. I. (2016). Adsorptive desulfurization of dibenzothiophene from fuels by rubber tyres-derived carbons: Kinetics and isotherms evaluation. *Process Safety and Environmental Protection*, *102*, 9–19. https://doi.org/10.1016/j.psep.2016.02.005

29. Shen, C., Gu, L., Chen, S., Jiang, Y., Huang, P., Li, H., Yu, H., Xia, D. (2022). Sewage sludge derived FeCl3-activated biochars as efficient adsorbents for the treatment of toxic As(III) and Cr(VI) wastewater. *Journal of Environmental Chemical Engineering*, *10*(6), 108575. https://doi.org/10.1016/j.jece.2022.108575

30. Siddique, A., Nayak, A. K., Singh, J. (2020). Synthesis of $FeCl_3$-activated carbon derived from waste Citrus limetta peels for removal of fluoride: An eco-friendly approach for the treatment of groundwater and bio-waste collectively. *Groundwater for*

*Sustainable Development*, *10*, 100339. https://doi.org/10.1016/j.gsd.2020.100339

31. Xiao, R., Yang, W., Cong, X., Dong, K., Xu, J., Wang, D., Yang, X. (2020). Thermogravimetric analysis and reaction kinetics of lignocellulosic biomass pyrolysis. *Energy*, *201*, 117537. https://doi.org/10.1016/j.energy.2020.117537

32. Xu, Z., Zhou, Y., Sun, Z., Zhang, D., Huang, Y., Gu, S., Chen, W. (2020). Understanding reactions and pore-forming mechanisms between waste cotton woven and $FeCl_3$ during the synthesis of magnetic activated carbon. *Chemosphere*, *241*, 125120. https://doi.org/10.1016/j.chemosphere.2019.125120

33. Yang, F., Zhang, S., Sun, Y., Du, Q., Song, J., Tsang, D. C. W. (2019). A novel electrochemical modification combined with one-step pyrolysis for preparation of sustainable thorn-like iron-based biochar composites. *Bioresource Technology*, *274*, 379–385. https://doi.org/10.1016/j.biortech.2018.10.042

34. Yaseen, M., Ullah, S., Ahmad, W., Subhan, S., Subhan, F. (2021). Fabrication of Zn and Mn loaded activated carbon derived from corn cobs for the adsorptive desulfurization of model and real fuel oils. *Fuel*, *284*, 119102. https://doi.org/10.1016/j.fuel.2020.119102

35. Yerdauletov, M. S., Nazarov, K., Mukhametuly, B., Yeleuov, M. A., Daulbayev, C., Abdulkarimova, R., Yskakov, A., Napolskiy, F., Krivchenko, V. (2023). Characterization of activated carbon from rice husk for enhanced energy storage devices. *Molecules*, *28*(15), 5818. https://doi.org/10.3390/molecules28155818

36. Zakaria, R., Jamalluddin, N. A., Abu Bakar, M. Z. (2021). Effect of impregnation ratio and activation temperature on the yield and adsorption performance of mangrove based activated carbon for methylene blue removal. *Results in Materials*, *10*, 100183. https://doi.org/10.1016/j.rinma.2021.100183

37. Zakir, M., Taba, P., Permatasari, N. U., Nurdin, M., Muliadi, M. (2025). Palm kernel shell based hydrothermal carbon for methylene blue removal in wastewater treatment: application of dual adsorption isothermal models. *Journal of Ecological Engineering*, *26*(7), 394–407. https://doi.org/10.12911/22998993/203741

38. Zazo, J. A., Bedia, J., Fierro, C. M., Pliego, G., Casas, J. A., Rodriguez, J. J. (2012). Highly stable Fe on activated carbon catalysts for CWPO upon FeCl3 activation of lignin from black liquors. *Catalysis Today*, *187*(1), 115–121. https://doi.org/10.1016/j.cattod.2011.10.003

39. Zhang, Z., Rao, X., Wu, Q., Wang, S., Chen, Y., Yang, X., Sun, X., Zhou, Q., Lu, P. (2025). Preparation of